Endo and Nagatani *Robomech J (2016) 3:20*
DOI 10.1186/s40648-016-0058-y

ROBOMECH Journal

RESEARCH ARTICLE Open Access

Assessment of a tracked vehicle's ability to traverse stairs

Daisuke Endo[1*] and Keiji Nagatani[2]

Abstract

In some surveillance missions in the aftermath of disasters, the use of a teleoperated tracked vehicle contributes to the safety of rescue crews. However, because of its insufficient traversal capability, the vehicle can become trapped upon encountering rough terrain. This may lead to mission failure and, in the worst case, loss of the vehicle. To improve the success rate of such missions, it is very important to assess the traversability of a tracked vehicle on rough terrains based on objective indicators. From this viewpoint, we first derived physical conditions that must be satisfied in the case of traversal on stairs, based on a simple mechanical model of a tracked vehicle. We then proposed a traversability assessment method for tracked vehicles on stairs. In other words, we established a method to evaluate whether or not a tracked vehicle can traverse the target stairs. To validate the method, we conducted experiments with an actual tracked vehicle on our simulated stairs, and we observed some divergences between our calculation and the experimental result. Therefore, we analyzed possible factors causing these divergences, estimated the influence of the factors quantitatively by conducting additional experiments, and identified the reasons for the deviation. In this paper, we report the above-described assessment method, the experiments, and the analyses.

Keywords: Tracked vehicle, Stairs, Stability, Traversing ability assessment

Background

Teleoperated small-sized tracked vehicles have two advantages compared to other vehicles: high traversability on rough terrain and a simple mechanism. Therefore, they are ideal for surveillance tasks to replace rescue crews in exploring hazardous environments in search and rescue missions. Well-known examples of tracked vehicles for practical use missions include Quince [1, 2] and Survey Runner [3]. These robots explored the buildings affected by the meltdown of the Fukushima Daiichi nuclear power plant. These robots provided significant information during surveillance missions, particularly related to damage inspection of plants and acquisition of dose distribution. However, in their last missions, both tracked vehicles got stuck in rough terrain and could not return. To prevent such situations, various approaches have been proposed to improve the usability of tracked vehicles; these include semi-autonomous control of subtracks [4–6] and consideration of robot stability in path planning [7]. However, no fundamental study has been conducted on assessing the ability of a tracked vehicle to traverse rough terrains from the point of view of the interaction between the tracks and the ground, directly.

To improve the success rate of such surveillance missions, a prior assessment is crucial. For example, in the case of surveillance missions in buildings, tracked vehicles are required to traverse stairs for moving to another floor. However, stair-climbing and stair-descending are obstacles that cause various problems in operation, and an assessment of traversability on stairs is important. Figure 1 shows the motion flow for a tracked vehicle traversing stairs for the stair-climbing case. The motion flow is divided into three steps:

(i) *Entering step* the motion state from contacting the first step of the stairs to finishing its traversal (Fig. 1(i)).
(ii) *Traversing step* the intermediate state between (i) and (iii) (Fig. 1(ii)), in which the pitch angle of the robot matches the inclination angle of the stairs.

*Correspondence: endo@frl.mech.tohoku.ac.jp
[1] Department of Aerospace Engineering, Graduate School of Engineering, Tohoku University, Aramaki-aza Aoba 468-1, Aoba-ku, Sendai 980-0845, Japan
Full list of author information is available at the end of the article

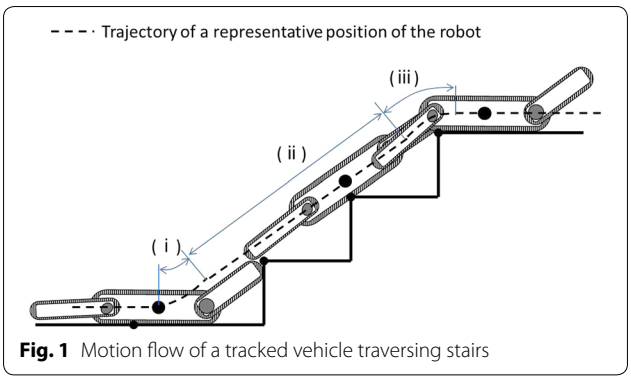

Fig. 1 Motion flow of a tracked vehicle traversing stairs

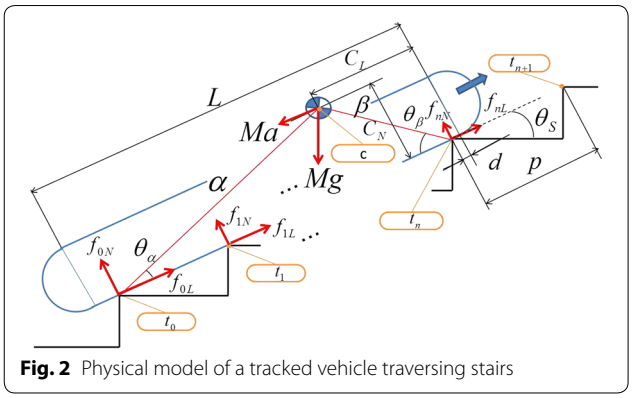

Fig. 2 Physical model of a tracked vehicle traversing stairs

(iii) *Landing step* the motion state from contacting the final step of the stairs to finishing its traversal (Fig. 1(iii)).

In previous research, Guo et al. stated that, to ensure traversability of a tracked vehicle on stairs, initially, the first step should be clear [8]. However, they did not consider the situation after the second step of the stairs-traversal. Jingguo et al. [9] conducted and examined a derivation of the physical condition to traverse stairs stably. However, they did not sufficiently validate its performance. Liu et al. proposed an online prediction system for monitoring the physical stability of a tracked vehicle [10], and Martens et al. proposed a practical control law to improve stability [11]. However, no previous study has verified a physical model to predict the stability of a tracked vehicle on stairs.

In this light, we develop a method for assessing whether or not a tracked vehicle can traverse stairs. Among the three steps [(i)–(iii)] described above, a physical condition of the entering step has been proposed and evaluated by Guo et al. [8]. However, after the robot completes the traversing step (ii), the landing step (iii) has not been considered from the point of view of traversability. Therefore, in this research, we focus on the traversing step (ii), and we propose an assessment method to evaluate, in advance, whether or not a tracked vehicle can traverse stairs.

Physical model of a tracked vehicle traversing stairs

Failure modes of tracked vehicles traversing stairs

First, to model a stair traversal of a tracked vehicle, we classified failure modes of a tracked vehicle that may occur during its traversal on stairs, and we derived physical conditions that cause each failure mode. Figure 2 shows a model of a tracked vehicle that has mass M in a two-dimensional plane as it traverses a flight of stairs. The angle of the stairs is θ_s, and the distance between the leading edges of adjacent steps (pitch between the edges of the stairs) is p. The length of the flat area of the track is L, and it has $n+1$ (where n is an integer greater than 2) contact points with the stairs. The contact points are defined as $t_0, t_1, \ldots, t_n$ from the bottom to the top. At each contact point, there are a tractive force f_{kL} and a vertical force f_{kN}. Here, k is an arbitrary integer between 0 and n. In addition, the robot is subject to an upward acceleration a along the stairs.

Figure 3 shows the state transition of the tracked vehicle while it traverses target stairs. Transitions occur when the number of contact points changes. In Fig. 3, we assume $np \leq L < (n+1)p$. The tracked vehicle traverses the stairs by transitioning through states A⟶B⟶C⟶D⟶A. When the track is in contact with the edge of a step, it is defined as state A. After that, it transitions to state B. When the track detaches from the edge of the step, it is defined as state C. After that, it transitions to state D.

To traverse the stairs successfully, a tracked vehicle should avoid the following three failure modes:

1 *Slipping* the case in which the tractive force F_{kL} is insufficient, and the track slides down on the stairs, as shown in Fig. 4.
2 *Falling backward* the case in which the robot's body tips over around the center t_0, the direction of rotation being counterclockwise, as shown in Fig. 5.
3 *Falling forward* the case in which the robot's body tips over around the center t_n, the direction of rotation being clockwise, as shown in Fig. 6.

The last mode (falling forward) occurs very rarely. It only occurs when the robot's centroid is located well forward in its body, and the robot is acts on by a large downward acceleration. In addition, this failure mode tends to cause less damage to the robot and its surrounding environment than the falling-backward mode.

This paper addresses and describes the physical conditions required to prevent the occurrence of these failure modes.

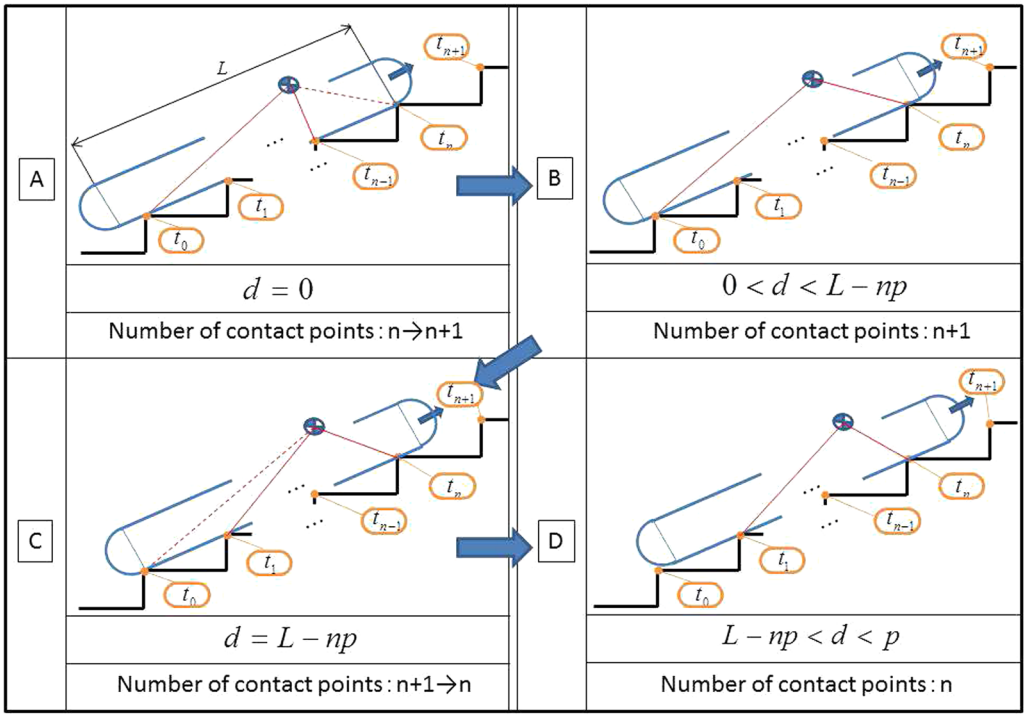

Fig. 3 State transitions of a tracked vehicle traversing stairs

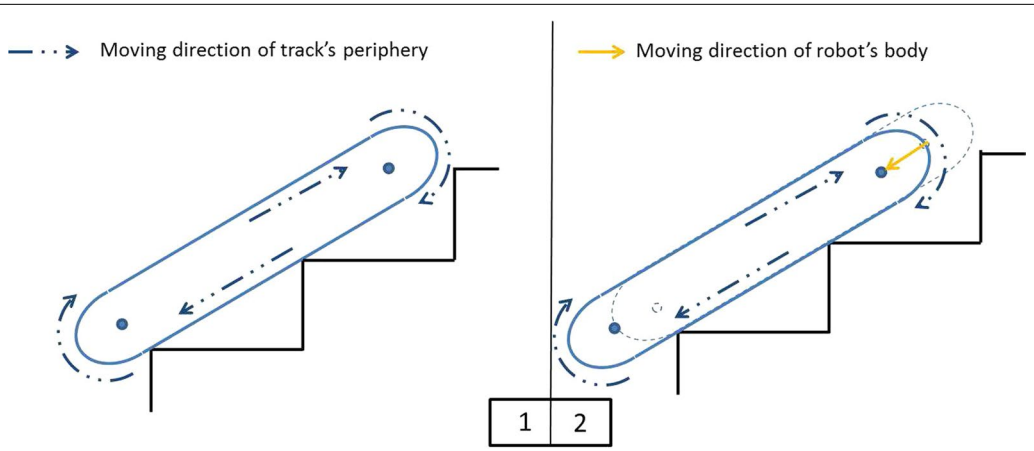

Fig. 4 Slipping mode

Slipping

When the traction force generated at the contact points between the tracks and the stairs does not exceed the static friction force, the tracked vehicle traverses the stairs without slipping. The condition is expressed by

$$\sum_{k=0}^{n} f_{kL} < \mu_S \sum_{k=0}^{n} f_{kN}, \tag{1}$$

where f_{kL} and f_{kN} are the tractive force and normal reaction force, respectively, at contact point t_k (where k is an arbitrary integer between 0 and n) and μ_S is the coefficient of friction between the tracks and the stairs. In this paper, it is assumed that μ_S has the same value at each contact point.

The equilibria of the lateral and longitudinal forces that describe the condition at which the robot is prevented from slipping can be expressed as

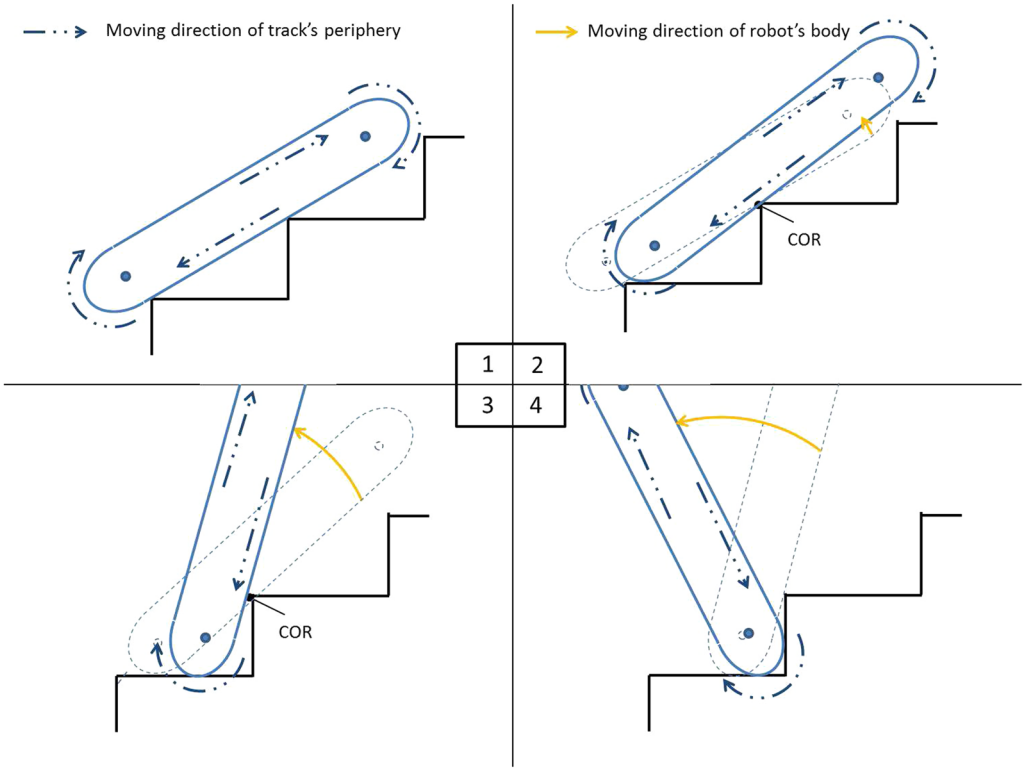

Fig. 5 Falling backward mode

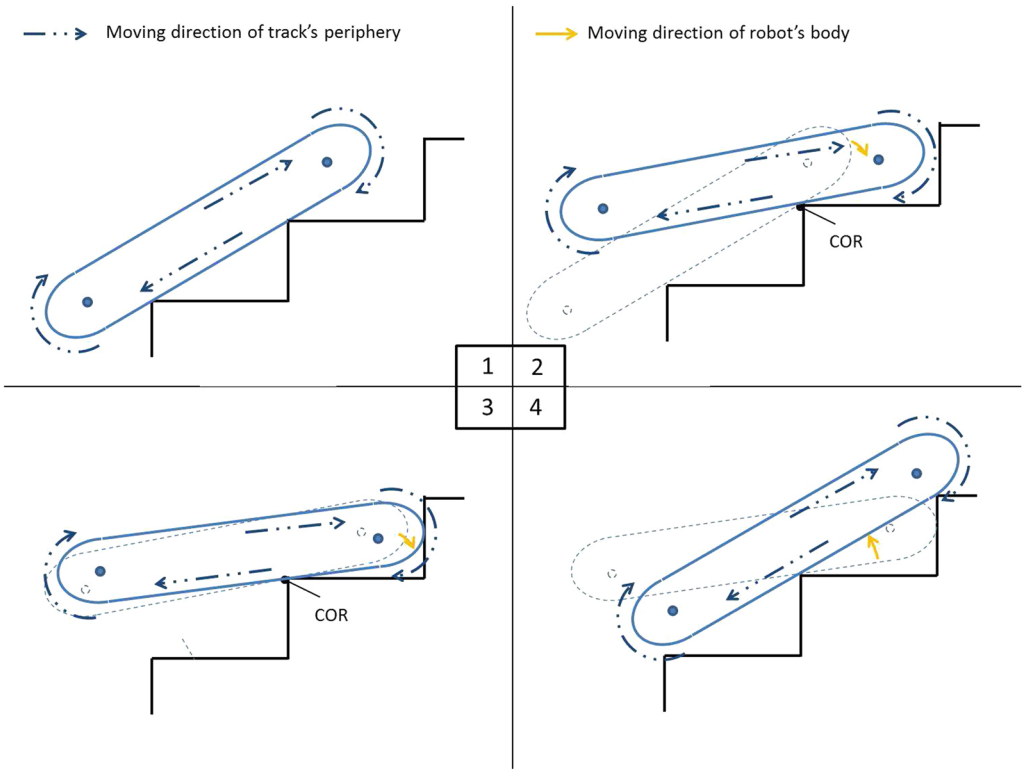

Fig. 6 Falling forward mode

$$Ma = \sum_{k=0}^{n} f_{kL} - Mg\sin\theta_s, \tag{2}$$

$$0 = \sum_{k=0}^{n} f_{kN} - Mg\cos\theta_s, \tag{3}$$

where M is the mass of the tracked vehicle, a is the lateral acceleration of the tracked vehicle, g is the gravitational acceleration, and θ_s is the angle of inclination of the stairs. Substituting Eqs. (2) and (3) into Eq. (1) and rearranging to obtain acceleration a gives

$$\begin{aligned} Ma + Mg\sin\theta_s &< \mu_s Mg\cos\theta_s. \\ \therefore a &< (\mu_s\cos\theta_s - \sin\theta_s)g. \end{aligned} \tag{4}$$

Falling backward

For a tracked vehicle to successfully traverse stairs, the summation of its angular moments must be zero. When a tracked vehicle has $n+1$ contact points without any rotation, as shown in Fig. 2, the balance of its moment around point t_0 can be described as follows:

$$\sum_{k=1}^{n} kpf_{kN} + Ma\alpha\sin\theta_\alpha - Mg\alpha\cos(\theta_s + \theta_\alpha) = 0, \tag{5}$$

where α is the distance between the centroid C and the contact point t_0, and θ_α is the angle formed by t_n and t_0 and C ($\angle t_n t_0 C$). When the robot rotates around the point t_0, there are no other contact points. Therefore, in this case, f_{kN} is equal to 0 (where k is an arbitrary integer between 1 and n) in Eq. (5), and the left-hand side of this formula becomes greater than 0. Thus, we can derive

$$\begin{aligned} Ma\alpha\sin\theta_\alpha - Mg\alpha\cos(\theta_s + \theta_\alpha) &> 0, \\ a &> \frac{\cos(\theta_s + \theta_\alpha)}{\sin\theta_\alpha} g. \\ \therefore a &> \left(\frac{\cos\theta_s}{\tan\theta_\alpha} - \sin\theta_s\right) g. \end{aligned} \tag{6}$$

The complementary condition to that described by Eq. (6) is required to prevent the robot from falling backward. Therefore, we derive

$$a \le \left(\frac{\cos\theta_s}{\tan\theta_\alpha} - \sin\theta_s\right) g. \tag{7}$$

With regard to $\triangle t_0 t_n C$, θ_α in Eq. (7) should satisfy

$$\theta_\alpha = \arccos\left(\frac{\alpha^2 + n^2p^2 - \beta^2}{2n\alpha p}\right), \tag{8}$$

$$\alpha = \sqrt{(d + np - C_L)^2 + C_N^2}, \tag{9}$$

$$\beta = \sqrt{(C_L - d)^2 + C_N^2}, \tag{10}$$

where α is the distance between centroid C and contact point t_0; β is the distance between centroid C and contact point t_n; d is the robot's progress, which is equal to 0 at state A in Fig. 3; C_L is the distance between the tip in the flat area of the track and the centroid C in the front–back direction; and C_N is the distance between the bottom of the track and the centroid C in the up–down direction.

Falling forward

As well as the falling-backward mode, when a tracked vehicle has $n+1$ contact points without any rotation, as shown in Fig. 2, the balance of its moments around point t_n can be described as follows:

$$\begin{aligned} &\sum_{k=0}^{n-1} (n-k)pf_{kN} - Ma\beta\sin\theta_\beta \\ &\quad - Mg\beta\cos(\theta_\beta - \theta_s) = 0. \end{aligned} \tag{11}$$

In the same way as the falling backward, the requirement to prevent the robot from falling forward is derived from

$$a \ge -\left(\frac{\cos\theta_s}{\tan\theta_\beta} + \sin\theta_s\right) g, \tag{12}$$

where θ_β is $\angle t_0 t_n C$. With regard to $\triangle t_0 t_n C$, θ_β is described by

$$\theta_\beta = \arccos\left(\frac{\beta^2 + n^2p^2 - \alpha^2}{2n\beta p}\right). \tag{13}$$

Traversing ability assessment method

Figure 7 shows a schematic diagram of the d–a plane. The vertical axis indicates the acceleration a of the robot, and the horizontal axis indicates the distance d that the robot progresses. The diagram includes (a) the state transition as a tracked vehicle traverses a flight of stairs and (b) the requirements for acceleration to prevent the robot from entering the failure modes described above. Furthermore, a_S, a_{r0} and a_{rn} are the marginal accelerations required to prevent the vehicle from slipping, falling backward, and falling forward, respectively. They are defined by

$$a_S = (\mu_s\cos\theta_s - \sin\theta_s)g, \tag{14}$$

$$a_{r0} = \left(\frac{\cos\theta_s}{\tan\theta_\alpha} - \sin\theta_s\right) g, \tag{15}$$

$$a_{rn} = -\left(\frac{\cos\theta_s}{\tan\theta_\beta} + \sin\theta_s\right) g. \tag{16}$$

These equations imply that slipping occurs when the acceleration of the robot is greater than a_S, falling

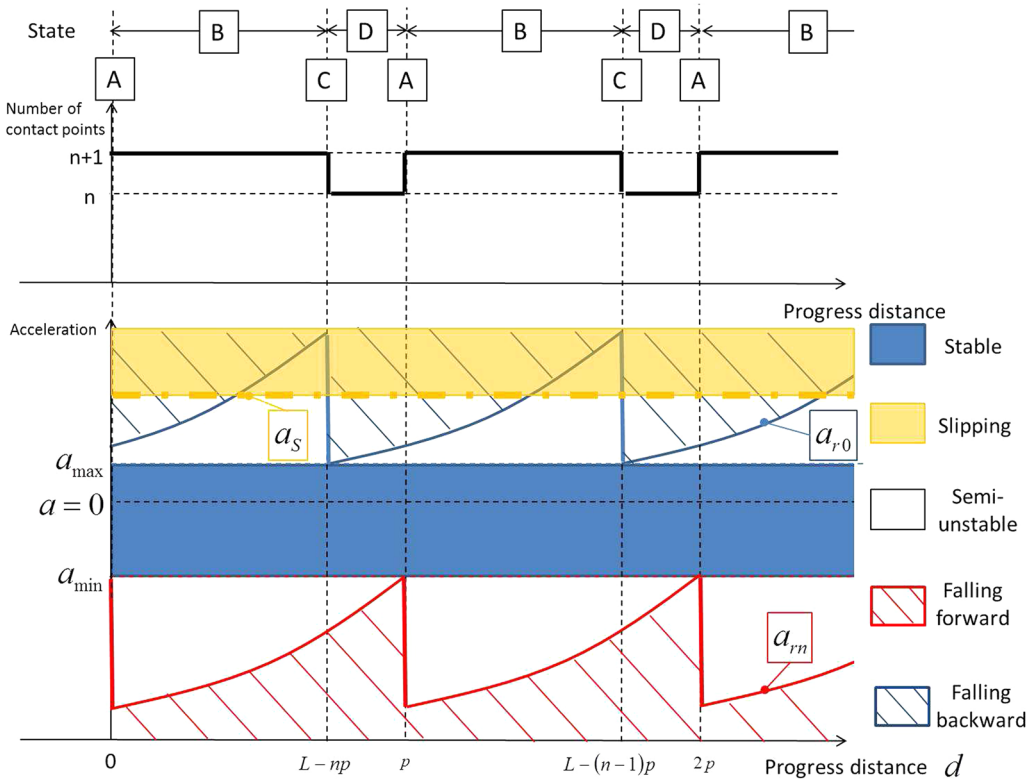

Fig. 7 Stability profile of a tracked vehicle traversing stairs

backward occurs when the acceleration of the robot is greater than a_{r0}, and falling forward occurs when the acceleration of the robot is less than a_{rn}. Here, $a_{\max}$ is defined as the lesser of the value of a_S and the minimum value attained by a_{r0}, and $a_{\min}$ is the maximum value attained by a_{rn}, as expressed, respectively, by

$$a_{\max} = \min(a_S, \min(a_{r0})), \tag{17}$$

$$a_{\min} = \max(a_{rn}). \tag{18}$$

The stability can be assessed based on the schematic diagram shown in Fig. 7. The d–a plane is divided into the following five areas, and the robot's stability can be categorized into one of the following states:

A. *Slipping area* When the acceleration a does not satisfy Eq. (4), the robot's body slips along the flight of stairs.
B. *Falling-backward area* When the acceleration a satisfies Eq. (4) but does not satisfy Eq. (7), the robot's body rotates around the contact point t_0.
C. *Falling-forward area* When the acceleration a does not satisfy Eq. (12), the robot's body rotates around the contact point t_n.
D. *Stable area* When the acceleration of the robot satisfies the condition $a_{\min} < a < a_{\max}$, it can traverse stairs without any slipping or rotation.
E. *Semi-unstable area* This area cannot be categorized as any of (A)–(D) above; however, it satisfies Eqs. (7) and (12). The robot can traverse the stairs.

The robot needs to be controlled to maintain its acceleration a in the semi-unstable area, according to the robot's position on the stairs. If the robot cannot control its acceleration accurately according to its position on the stairs, this area should be considered unstable. In this case, the robot should be controlled in the stable area (D). Additionally, note that the robot slips prior to rotation if the acceleration a does not satisfy Eqs. (4) and (7).

In other words, the robot can traverse the stairs without any slipping or rotation if its acceleration is controlled in the stable area (D).

Case study

We conducted a case study with a tracked vehicle, called "Kenaf" [12, 13], that traverses stairs using the traversability assessment method described in the previous section. In this case study, we assumed that the robot's

speed was constant (acceleration $a = 0$). There were two reasons for this assumption. One is because it is difficult for Kenaf to maintain its acceleration when moving on stairs owing to the power restriction of its actuators. The other is that the increase and decrease in acceleration are equivalent to that of the inclination of stairs based on the physical model shown in Fig. 2. In addition, Kenaf originally has two main tracks and four sub-tracks. However, to improve the accuracy of the verification tests described in the next section, the robot's mechanical system should be simple. Therefore, we used Kenaf without all of its sub-tracks; only the two main tracks were used in this case study (Fig. 8). The physical parameters of the robot, as used for the calculation, are listed in Table 1.

Kenaf has multiple convex-shaped grousers made of chloroprene rubber on the surface of the tracks (Fig. 9). Therefore, the friction between the tracks and the ground is sufficient to prevent slipping, and falling backward occurs prior to slipping on stairs with large inclinations in the preliminary experiments. In other words, in case of $a_S > \min(a_{r0})$, slipping does not occur. Furthermore, falling forward did not occur at constant speed. Consequently, we only consider the falling-backward phenomenon for assessing problems related to the shape of the stairs for Kenaf.

The shape of the stairs can be described by two parameters: the angle of inclination of the stairs, θ_s, and the pitch between the edges of the stairs, p. The condition for whether falling backward occurs (described as "margin" in this paper) in the θ_s–p plane can be derived by substituting $a = 0$ in Eqs. (7)–(10). This margin can be described by the following set of equations:

$$\theta_s^{sup} = \frac{\pi}{2} - \theta_{\alpha C}, \tag{19}$$

$$\theta_{\alpha C} = \arccos\left(\frac{\alpha_C^2 + (n-1)^2 p^2 - \beta_C^2}{2(n-1)\alpha_C p}\right), \tag{20}$$

Table 1 Robot specifications

Parameter	Symbol	Value [mm]
Centroid position in front–back direction	C_L	196
Centroid position in up–down direction	C_N	71
Length of flat area	L	470

$$\alpha_C = \sqrt{\{d_C + (n-1)p - C_L\}^2 + C_N^2}, \tag{21}$$

$$\beta_C = \sqrt{(C_L - d_C)^2 + C_N^2}, \tag{22}$$

$$d_C = L - np. \tag{23}$$

These new symbols in Eqs. (19)–(23) can also be denoted like as Fig. 10. Figure 11 shows the predicted margin obtained by substituting Kenaf's parameters (Table 1) into Eqs. (19)–(23). This means that, theoretically, the robot falls backward in the area on the right, but not in the area on the left in the plane bounded by the solid line.

Verification test

To verify the traversability assessment method, we conducted verification tests to compare with the predicted margin obtained in the previous section.

Equipment

Tracked vehicle

For this test, we used Kenaf (Fig. 8).

Simulated stairs

We fabricated the simulated stairs shown in Fig. 12. The setup allowed us to change the inclination θ_s of the stairs to any value between 0° and 70°, and the pitch between

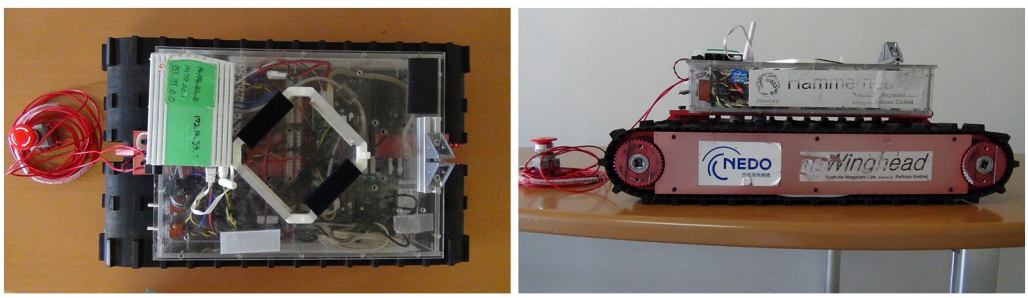

a Top view b Side view

Fig. 8 The target tracked vehicle used in our verification test

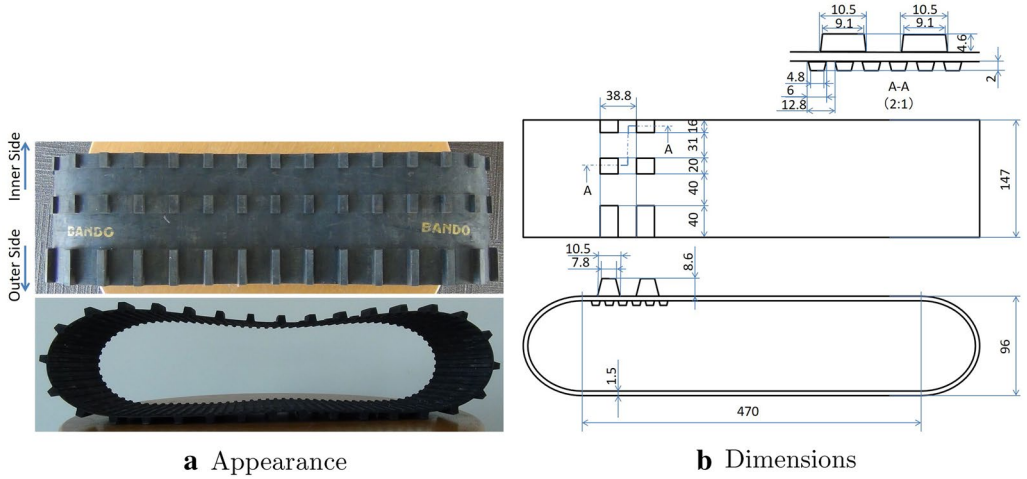

Fig. 9 Shape of the main track

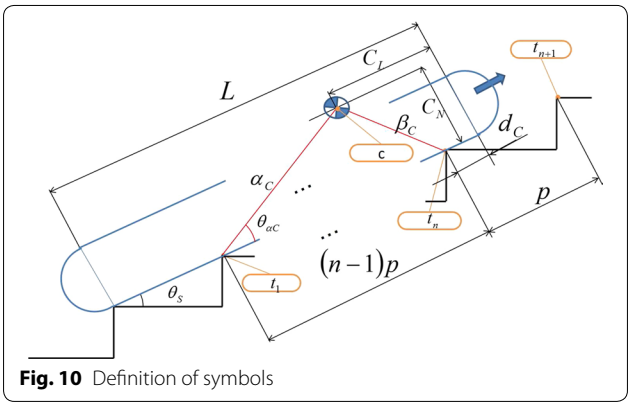

Fig. 10 Definition of symbols

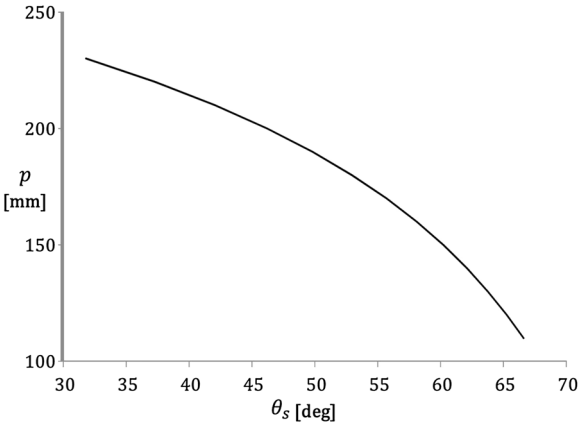

Fig. 11 Predicted margin of Kenaf

the edges of the stairs, p, could be changed to any value up to 2400 mm. The inclination and the pitch between the edges of the stairs were adjusted by changing the positions of fixing nuts.

Test procedure

We conducted traversal tests under different (θ_s, p) conditions. For each trial, the tracked vehicle was placed on the simulated stairs and operated to climb up vertically to the end of the stairs at a constant speed, 100 mm/s (acceleration $a = 0$). This value of speed is the upper limit for the Kenaf to keep on steep stairs. We then observed its behavior and judged whether or not falling backward occurred. At the tip of the robot, a safety tether was attached to prevent the robot from falling and crashing. The pitch between the edges of the stairs, p, was changed to four different values—150, 180, 200 and 220 mm—and the inclination of the stairs θ_s was changed discretely. At each pitch between the edges of the stairs, we evaluated the marginal inclination θ_s^{sup} above which falling backward occurred. We performed five trials under the same conditions.

Test results

Figure 13 shows the results of the above tests. In the graph, the symbols have the following meaning:

◯: The robot did not fall at any time.
×: The robot fell down all five times.
△: The robot fell backward sometimes. The index represents the frequency of falling backward.

The solid line in this graph is the same as the solid line in Fig. 11.

Fig. 12 Changeable stairs simulation

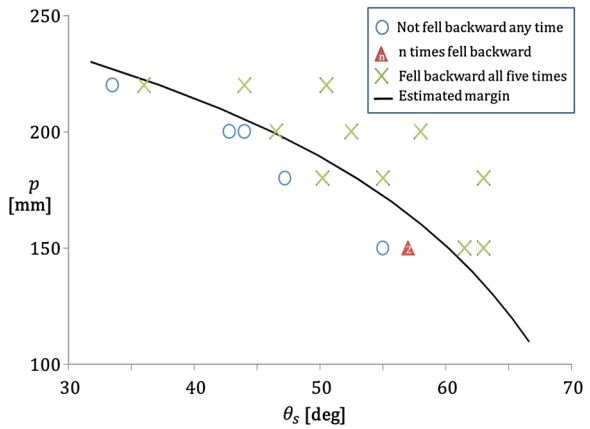

Fig. 13 Experimental results

Discussion

The results of the tests described in the previous section are in good agreement with the predicted values in those areas where the inclination θ_s is relatively small. These results indicate that the falling-backward phenomenon predominantly depends on the relation between the robot's centroid and the shape of the stairs, as described in Eqs. (19)–(23). This fact is the good evidence of necessity to consider the centroid position exactly, in case not only for stability assessment but also stage of design for the tracked vehicles. However, in those areas where θ_s is large, the predicted values diverged from the measured values. The largest difference was observed when $p = 150$ mm: the robot fell down at 55.0°–57.0° in the experiment; however, the predicted margin was 60.2°. Figure 14 shows the behavior of the robot when the robot traverses a flight of stairs for which $\theta_s = 44.0°$ and $p = 200$ mm. The falling-backward phenomenon did not occur in this case; however, the robot's body started to exhibit a swinging motion, as shown in Fig. 14(2). This situation occurred when the edge of the track detached from the contact point. Moreover, the robot satisfies Eq. (7) at this instant, because the projecting point of the robot's centroid is located within the polygon formed from the contact points without a detaching point [14]. Therefore, the other phenomenon must have occurred exactly when the edge of the track detached. In the next section, we discuss the reasons for this divergence.

Deformation of the track

Generally, a tracked vehicle, including Kenaf, has multiple grousers across the surface of its tracks to increase the friction between the track's surface and the ground, thereby preventing the track from slipping. Typically, for small tracked vehicles, the tracks are made of a nonrigid material.

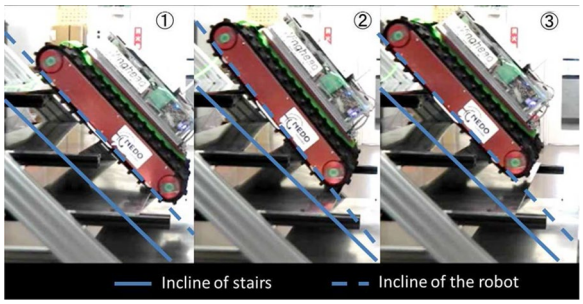

Fig. 14 Robot's behavior when traversing stairs ($\theta_s = 44.0°$, $p = 200$ mm)

Therefore, bending deformation of the track occurs at the point where the grouser comes into contact with the edge of the stairs, particularly at the lowermost contact point. As a result, the deformation increases the pitch angle of the robot's body. When the load-sharing ratio at the bottom of the contact point is maximized, the pitch angle of the body is also maximized, as shown in Fig. 15. In this paper, we describe the amount of increase in the pitch angle of the robot's body caused by the above reason as θ_M. To eliminate the influence of this factor, we measured the maximum increment of the pitch angle θ_d at $p = 150$, 180 and 200 mm. In each condition, the angle of inclination of the stairs was approximately marginal to falling backward.

Figure 15 shows a side view of the robot's state on stairs with $(p, \theta_s) = (150 \text{ mm}, 56.8°)$. In this case, the result was 2.6° greater than the inclination angle of the stairs. Therefore, we concluded that the deformation of the track grousers is one of the reasons for the divergence.

In this paper, we evaluated the influence of the deformation factor for Kenaf only (Fig. 16). However, the amount of deformation is determined by the rigidity of the tracks,

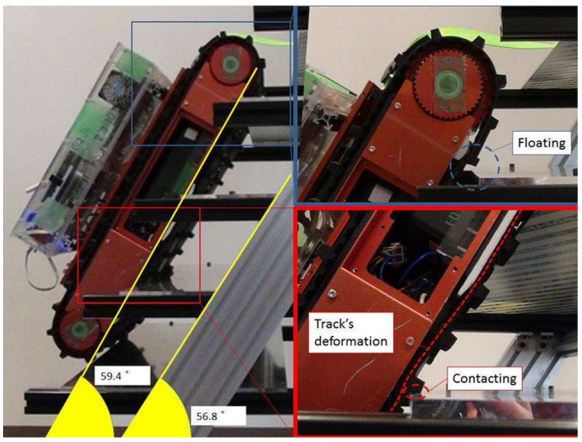

Fig. 15 Increase of the pitch angle of the robot caused by track deformation

the relative positions of the centroid of the robot, and the edge of the stairs. This deformation problem is common and can emerge for various tracked vehicles. Therefore, our proposal and verification tests are applicable not only to this particular robot but to tracked vehicles in general.

Lowest contact point angular moment generation by grousers

When the lowermost contact point of a track detached from the edge of a step, it takes some time because of the action of the grouser. During this period, the grouser causes the circular part of the track to move, and it generates an angular moment that pushes the lower part of the robot's body down, as shown in Fig. 17(3). The moment at the lowest contact point angular moment is abbreviated as LCM in this paper. This period is very short, but it increases the pitch angle of the robot's body. When the robot is just about

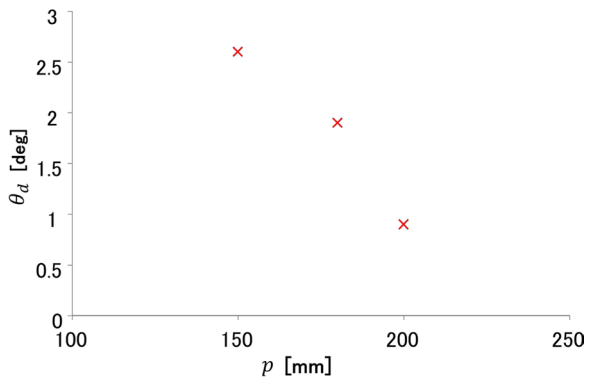

Fig. 16 Measurement results for θ_d, between the pitch angle of the robot and the pitch p of stairs

to tip over, the LCM may provide the impetus for the robot to fall backward.

However, with regard to the descent of a tracked vehicle, an LCM is not generated owing to the relative positions of the grouser and the edge of the stairs (Fig. 18). Therefore, the influence of the LCM on the divergence can be evaluated by comparing the marginal angles for the ascent and descent of the same stair configuration. Figure 19 shows the results of these additional tests. In this figure, the vertical axis θ_M is the difference between the marginal angle for descending and the marginal angle for ascending. The error range in Fig. 19 describes the variance in the experiments, which were conducted five times for each condition.

The tests were conducted at three conditions: $p = 150$, 180 and 200 mm. In each condition, the marginal angle for descending was larger than that for ascending. Focusing on the result of $p = 150$ mm, we see that θ_M was between 1.2° and 2.6°. We can recognize this value as the influence of the LCM on the divergence between the theoretical and the measured marginal angles.

Summary of discussion

Figure 20 summarizes the above discussion. The process whereby the robot falls backward is explained as follows:

1. When the lowermost contact point is located under a flat part of the track, the tracked vehicle moves parallel to the stairs, keeping the summation of its angular moments at zero.
2. After the lowermost contact point reaches the end of the flat area, the tractive force resulting from the contact of the grouser affects the robot body tangentially to the circular part of the track. According to the tractive force, the LCM continues to affect the robot until the grouser completely separates from the edge of the stair.
3. When the load-sharing ratio at the bottom of the contact point is maximized, the elevation angle is also maximized. As a result, the location of the centroid moves backward.
4. When the lowermost contact point separates completely from the edge of the stairs, the projecting point of the centroid is located more toward the rear of the robot than at the rotation center.

Given the above results, we conclude that falling backward can actually happen relatively easily in comparison with the results of our calculations, particularly when the stairs are steep. Figure 21 shows the result obtained from Fig. 13, reflecting the results shown in Figs. 16 and 19. We confirmed that the prediction accuracy for falling

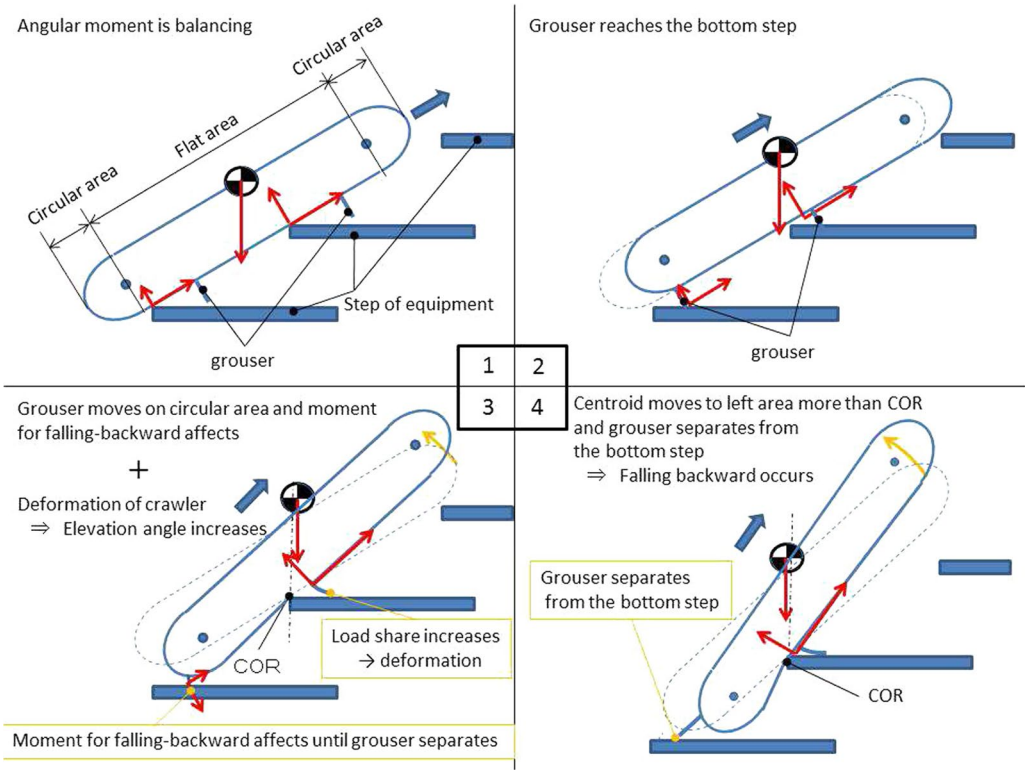

Fig. 17 Falling-backward mode affected by track deformation and rib

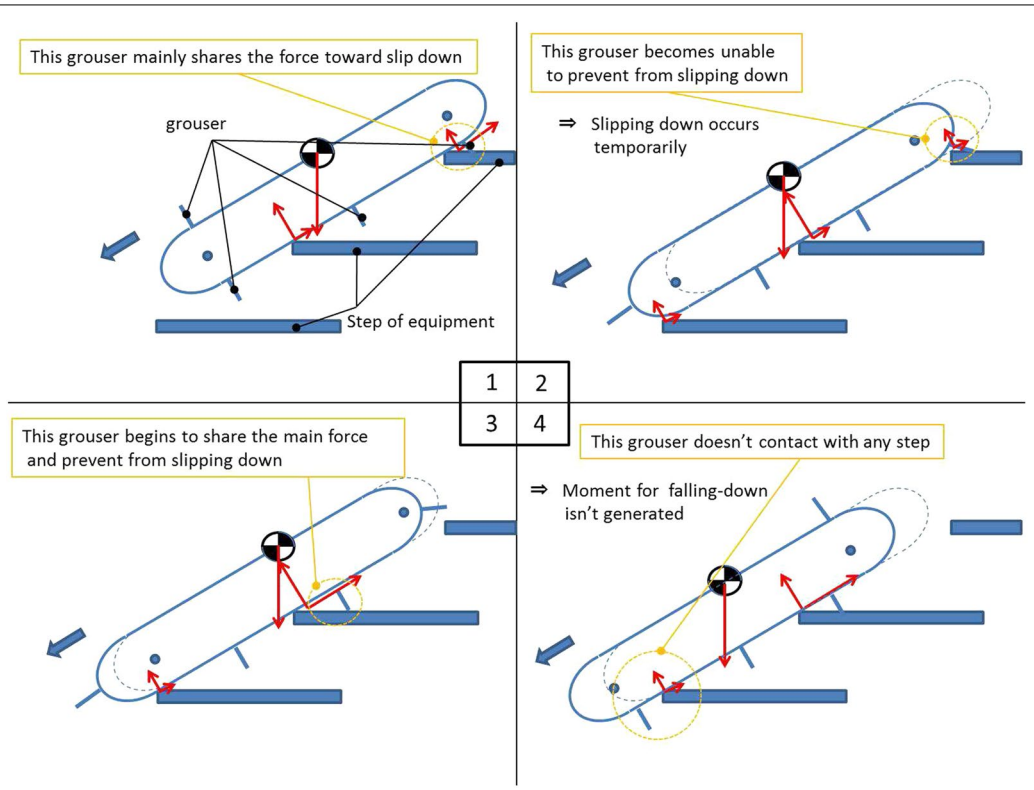

Fig. 18 State transitions of a tracked vehicle going downstairs

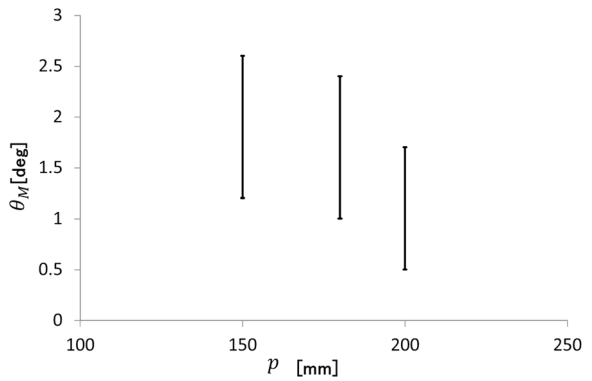

Fig. 19 Difference between marginal inclines for ascent and descent of Kenaf

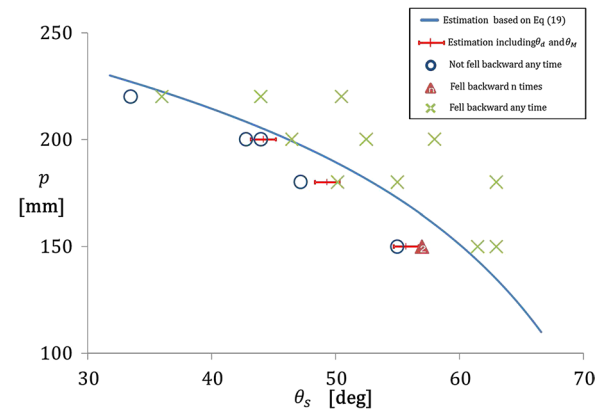

Fig. 21 Comparison of the predicted margin and the modification method

backward improves upon including the effects of θ_d and θ_M in Eq. (19).

The above results for assessing a robot's ability to traverse the stairs are going to be improved. In other words, modification from Eqs. (19) to (24) is effective using the parameters described in Eqs. (20)–(23):

$$\theta_s^{sup} = \frac{\pi}{2} - \theta_{x\alpha} - \theta_d - \theta_M. \tag{24}$$

As a supplement, the data denoted by red points with error range in Fig. 21 are the estimation results based on Eq. (24).

Conclusion and future work

Based on a mechanical model, we have derived the physical conditions under which a tracked vehicle can traverse stairs without falling, and we have performed verification tests using a tracked vehicle to clarify the backward-falling failure mode. As a result, for stairs with relatively small inclination, it is possible to assess whether they can be traversed by the robot based on the robot's centroid, the length of track, inclination, and the pitch between the edges of the stairs. However, for stairs with very large inclination, we confirmed that the robot fell backward more easily than indicated by our calculations. Therefore,

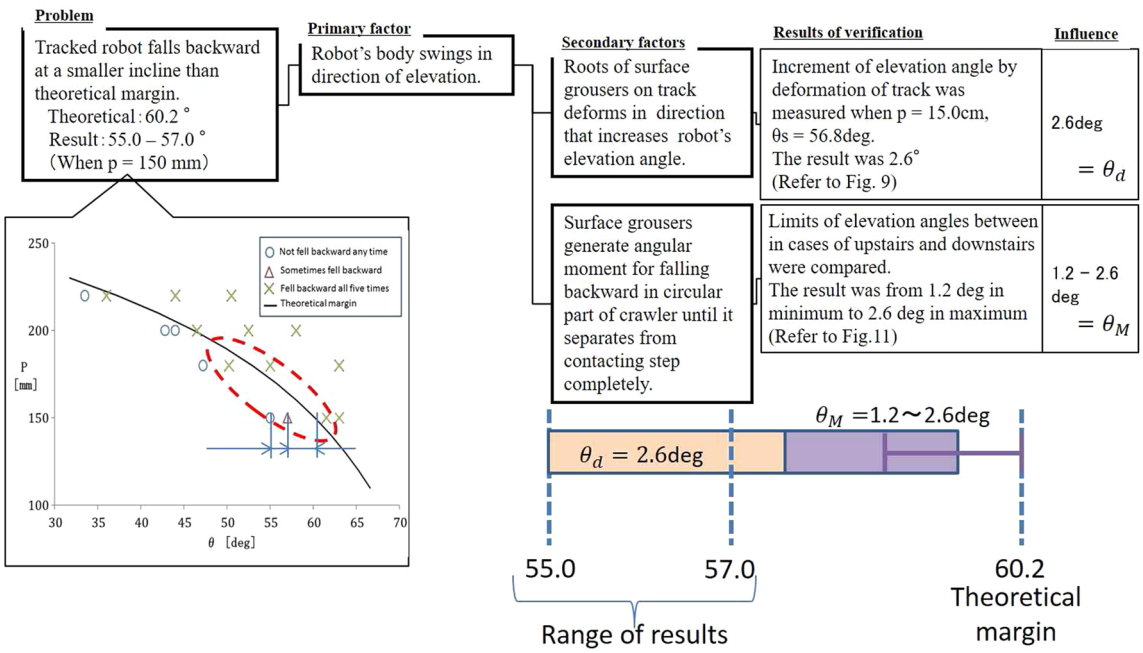

Fig. 20 Summary of cause investigation

we conducted additional experiments and identified two primary factors for the robot to tip: the deformation of the tracks caused by the increase of load sharing at the lowermost contact point and the influence of the LCM generated by the grouser that maintains contact when it moves along the circular part of the track. The influence of each primary factor was evaluated quantitatively. Conclusively, we found a more accurate method to assess the robot's traversal ability described in Eq. (24).

The method requires not only the parameters of the configuration of the target tracked vehicle and the stairs but others as well. We can expect that the effect of θ_d can be estimated by mechanical analysis, including some factors such as the shape of stairs, the centroid of the robot, and the shape and mechanical conductance of the tracks. θ_M is determined by the interactive force between the tracks and the stairs, and it may also be affected by the grouser shape. However, quantitative methods to estimate the effects of the grouser shape have not been established yet. Therefore, more fundamental experiments and analyses are required to account for these effects.

This research covers only stairs with a constant inclination and a pitch between the contact points. In future work, we will extend the derived physical model to general terrains whose inclination and pitch between contact points are not constant. In addition, we will establish an assessment method of slipping phenomena to determine, in advance, whether the robot can traverse the terrain.

Authors' contributions

DE contributed to the conception, experimental design, acquisition and interpretation of data, and writing of the manuscript. KN took part in the conception and in revising the manuscript. Both authors read and approved the final manuscript.

Author details

[1] Department of Aerospace Engineering, Graduate School of Engineering, Tohoku University, Aramaki-aza Aoba 468-1, Aoba-ku, Sendai 980-0845, Japan. [2] New Industry Creation Hatchery Center, Tohoku University, Aramaki-aza Aoba 6-6-10, Aoba-ku, Sendai 980-8579, Japan.

Acknowledgements

This work was supported in part by a Grant-in-Aid for JSPS Fellows (No. 16J2554). Also, we gratefully acknowledge the work of past and present members of our laboratory, especially, Mr. Kai Kudo, contributing to some interpretation of data. Also, we would like to thank Editage (http://www.editage.jp) for English language editing.

Competing interests

The authors declare that they have no competing interests.

Received: 7 June 2016 Accepted: 22 August 2016
Published online: 13 September 2016

References

1. Yoshida T, Nagatani K, Tadokoro S, Nishimura T, Koyanagi E (2012) Improvements to the rescue robot Quince toward future indoor surveillance missions in the Fukushima Daiichi Nuclear Power Plant. In: Preprints of the 8th International Conference on field and service robotics, vol 80. Springer, Berlin, Heidelberg
2. Nagatani K, Kiribayashi S, Okada Y, Tadokoro S, Nishimura T, Yoshida T, Koyanagi E, Hada Y (2011) Redesign of rescue mobile robot Quince—toward emergency response to the nuclear accident at Fukushima Daiichi Nuclear Power Station on March 2011. In: Proceedings of the 2011 IEEE International workshop on safety, security and rescue robotics, pp 13–18. IEEE, USA
3. Tokyo Electric Power Co., Inc. (2012) Guide to citing Internet sources. http://www.tepco.co.jp/en/nu/fukushima-np/images/handouts_120417_03-e. Accessed 1 Mar 2012
4. Okada Y, Nagatani K, Yoshida K, Yoshida T, Koyanagi E (2010) Shared autonomy system for tracked vehicles to traverse rough terrain based on continuous three-dimensional terrain scanning. In: Proceedings of the 2010 IEEE/RSJ International Conference on intelligent robots and systems, pp 357–362. IEEE, USA
5. Ohno K, Morimura S, Tadokoro S, Koyanagi E, Yoshida T (2007) Semi-autonomous control system of rescue crawler robot having flippers for getting over unknown-steps. In: Proceedings of the 2007 IEEE/RSJ International Conference on intelligent robots and systems, pp 3012–3018. IEEE, USA
6. Ohno K, Takeuchi E, Chun V, Tadokoro S, Yuzawa T, Yoshida T, Koyanagi E (2009) Rollover avoidance using a stability margin for a tracked vehicle with sub-tracks. In: Proceedings of the 2009 IEEE International workshop on safety, security, and rescue robotics, pp 1–6. IEEE, USA
7. Magid E, Tsubouchi T, Koyanagi E, Yoshida T (2010) Static balance for rescue robot navigation: losing balance on purpose within random step environment. In: Proceedings of the 2010 IEEE/RSJ International Conference on intelligent robots and systems, pp 349–356. IEEE, USA
8. Guo Y, Song A, Bao J, Zhang H, Tang H (2010) Research on centroid position for stairs climbing stability of search and rescue robot. Int J Adv Robot Syst 7(4):24–30
9. Liu J, Wang Y, Ma S, Li B (2005) Analysis of stairs-climbing ability for a tracked reconfigurable modular robot. In: Proceedings of the 2005 IEEE International workshop on safety, security and rescue robotics, pp 36–40. IEEE, USA
10. Liu Yugang, Liu Guangjun (2009) Track-stair interaction analysis and online tipover prediction for a self-reconfirable tracked mobile robot climbing stairs. IEEE/ASE Trans Mech 14(5):528–538
11. Martens JD, Newman WS (1994) Stabilization of a mobile robot climbing stairs. In: Proceedings of the International Conference on robotics and automation, pp 2501–2507. IEEE, USA
12. Yoshida T, Koyanagi E, Tadokoro S, Yoshida K, Nagatani K, Ohno K, Tsubouchi T, Maeyama S, Noda I, Takizawa O, Hada Y (2007) A high mobility 6-crawler mobile Robot "Kenaf." In: Proceedings of the 4th International workshop on synthetic simulation and robotics to mitigate earthquake disaster, p 38
13. Ohno K, Tadokoro S, Nagatani K, Koyanagi E, Yoshida T (2010) Trials of 3D Map construction using the tele-operated tracked vehicle Kenaf at Disaster City. In: 2010 IEEE International Conference on robotics and automation, pp 2864–2870
14. Hirose S et al Normalized energy stability margin: generalized stability criterion for walking vehicles. In: Proceedings of the International Conference on climbing and walking robots, pp 71–76. Springer, Berlin, Heidelberg